Crystalline Inverted Membranes Grown on Surfaces by Electrospray Ion Beam Deposition in Vacuum

Stephan Rauschenbach, Gordon Rinke, Nikola Malinowski, R. Thomas Weitz, Robert Dinnebier, Nicha Thontasen, Zhitao Deng, Theresa Lutz, Pedro Martins de Almeida Rollo, Giovanni Costantini, Ludger Harnau, and Klaus Kern*

The properties of organic thin film devices such as displays or solar cells critically depend on the homogeneity, cleanliness and crystallinity of the organic layers they are made of.[1] Vapor deposition in vacuum is the technology of choice for fabricating such films since it allows controlling the internal structure of the materials at the microscopic level. However, this technique is not applicable to a large fraction of functional organic molecules that cannot enter the gas phase due to their thermal instability.

Electrospray ionization (ESI) is capable of creating intact gas phase ions of such nonvolatile molecules, thereby greatly extending the scope of mass spectrometry.[2] Moreover, electrospray ion beam deposition (ES-IBD) has recently been developed as a method capable to deposit nonvolatile molecules on surfaces in vacuum.[3–5] Due to the low intensity of ESI sources, morphology and microscopic structure of films grown by molecular ion beams were rarely the subject of investigation and so far, neither multilayered nor crystalline growth could be evidenced.[6–8]

While neutral atoms and molecules from thermal sources (25–100 meV) are used in conventional thermal evaporation, ES-IBD employs charged molecules with hyperthermal energies (2–100 eV). These differences have the potential to significantly change the molecule-surface and intermolecular interactions as well as the thermodynamics of the film growth. Thus, the question must be raised whether crystalline growth with ES-IBD is possible at all and how the characteristics of the charged, hyperthermal molecular beam influence the crystal structure and morphology of the deposited films. Moreover, the fact that ion beams can be manipulated by electric fields might offer additional leverage to control the film growth.

In the following we show that ES-IBD[3,4,6] is a versatile method for the vacuum growth of crystalline organic films, whose constituents are not compatible with conventional, evaporation-based organic molecular beam epitaxy. As a model system we use sodium dodecyl sulfate (SDS), a nonvolatile organic salt widely employed as surfactant. Ion beams of large, multiply charged clusters of SDS, controlled with respect to composition, flux and energy, are deposited on silicon oxide, graphite and copper surfaces by ES-IBD under (ultra-) high vacuum conditions. Cluster beams allow a high flux deposition by which stable and homogenous multilayered films can be formed that are characterized by scanning probe microscopy (SPM) and X-ray powder diffraction (XRPD). Phases consisting of molecules in flat laying and inverted membrane configuration are found. Their basic structural motive is always a head-to-head and tail-to-tail configuration characteristic of amphiphilic molecules. This study paves the way for a chemically controlled vacuum growth of novel thin films based on nonvolatile materials. The fabrication of crystalline coatings from polymers,[9] proteins[2] or coordination compounds[8] can be envisioned.

Figure 1a outlines the different steps of an ion beam deposition experiment. A key advantage of ES-IBD is the capability to fully characterize the ion beam before deposition with respect to kinetic energy, ion current, chemical composition and purity.[4] First, positively charged SDS ion beams were created by electrospray ionization (ESI) and characterized in situ by time-of-flight mass spectrometry (TOF-MS). These SDS ion beams were guided by transfer ion optics to the deposition target,[4] which was either graphite or silicon oxide (SiO_x), later characterized ex situ using AFM, or a single crystal Cu(001) surface characterized in situ with STM. An incidence energy of 5–25 eV per charge is set by applying a voltage to the sample. Deposition currents of up to 250 pA were measured at the sample position, monitored in real time during the deposition.

Mass spectrometry shows that ESI generates charged clusters of SDS (sketched in Figure 1a) from a 10 mM solution of the molecules in water and methanol. A typical mass spectrum is displayed in Figure 1b. The size of the clusters (n = number

Dr. S. Rauschenbach, G. Rinke, Dr. N. Malinowski,[+] Dr. R. T. Weitz, Prof. R. Dinnebier, Dr. N. Thontasen, Dr. Z. Deng, Dr. T. Lutz, P. M. de Almeida Rollo, Prof. G. Costantini, Prof. K. Kern
Max-Planck-Institute for Solid State Research
Heisenbergstr. 1, D-70569 Stuttgart, Germany
E-mail: s.rauschenbach@fkf.mpg.de
Prof. G. Costantini
Department of Chemistry
University of Warwick
Gibbet Hill Road, CV4 7AL Coventry, UK
L. Harnau
Max-Planck-Institute for Intelligent Systems
Heisenbergstr. 3, 70569 Stuttgart Germany
and Institut für Theoretische und Angewandte Physik
Universität Stuttgart
Pfaffenwaldring 57, 70569 Stuttgart, Germany
Prof. K. Kern
Physique de la matière condensée Ecole Polytechnique Fédérale de Lausanne
CH-1015 Lausanne, Switzerland
[+] Present Address: Central Laboratory of Photoprocesses, Bulgarian Academy of Sciences, 1113 Sofia, Bulgaria

DOI: 10.1002/adma.201104790

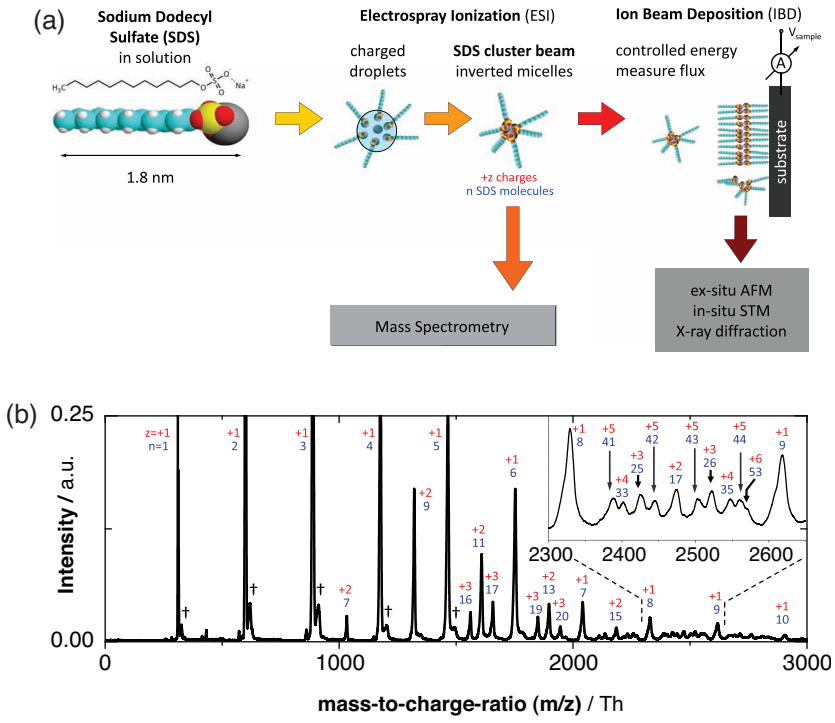

Figure 1. a) Scheme of the IBD Experiment. Molecular structure of the SDS molecule, $Na^+[SO_4(CH_2)_{11}CH_3]^-$, m = 288 u, Na - gray, S - yellow, O - red, C - blue, H - white. Formation of inverse micelle SDS clusters by electrospray ionization. Layer formation on the substrate in vacuum. b) ESI-TOF mass spectrum of a SDS cluster beam from a 10 mM solution as used for deposition. The peaks are labeled with the charge state *z* (red) and number of SDS molecules *n* (blue) of the corresponding cluster ion. The inset magnifies a part of the mass spectrum in which high charge state clusters with a high mass are clearly identified.

of SDS molecules) and their charge state (up to $z = 6$) are indicated for each peak by blue and red numbers, respectively. In analogy to other charged surfactant aggregates it can be expected that SDS clusters in vacuum have an inverse micelle configuration, in which the hydrophobic part of the molecule forms a shell around an ionic core.[10] Limited by the resolution of our TOF-MS, clusters were observed up to m/z-values of 7000 Th with charges up to $z = 6$. The absence of contamination or solvent molecules is evidenced by the fact that all peaks can be identified as positively charged clusters composed of SDS with one or several excess Na^+ as charge carriers. The purity of larger clusters can be confirmed through their low m/z fragments, which do not show signs of contamination. Satellite peaks next to intense, single charged peaks (marked with † in Figure 1b) are an indication of a small concentration of K^+ ions.

Essential to each deposition technique is the control of the material flux. In case of ES-IBD this can be done conveniently by measuring the deposition current. However, for cluster beams, the average mass-to-charge-ratio has to be determined to relate the accumulated charge to the amount of material; a task which is not trivial for beams containing many different cluster ions. Our analysis of the well resolved charge states $z = 1$–5 of the SDS mass spectra up to $m/z = 3500$ Th yields an average cluster size of approximately 5 molecules per charge.[11] We find that in this range small, lowly charged clusters contribute most of the electrical current and appear with high intensity in the mass spectra, but the major amount of SDS molecules is contained in large, highly charged clusters of low mass-spectral abundance. The extrapolation of this trend to higher m/z suggests that the average cluster size and, hence, the material flux is probably very large, because the unresolved intensity beyond 3500 Th was not included in this analysis. More advanced mass-spectrometers than the linear TOF in our apparatus could resolve larger clusters and thus allow for a more precise measurement of the material flux before deposition.[12]

Alternatively, ES-IBD can be used to overcome this limitation of our mass spectrometer: the amount of material found on the surface after deposition can be measured and used to determine the average cluster size in the beam independent from mass spectrometry. Moreover, such an analysis includes all clusters contained in the ion beam and thus offers a possibility to quantify the deposition rate. The precise knowledge of the molecular structure of SDS films is the prerequisite to extract the total amount of deposited material from the surface coverage observed by atomic force microscopy (AFM). The time-integrated ion current measured on the sample yields the deposited charge. For the given conditions in our deposition experiments these quantities allow an estimate for the average cluster m/z-ratio of 5000 ± 900 Th, which corresponds to approximately 17 molecules per charge; as expected much more than the number of 5 molecules per charge roughly estimated from TOF-MS measurements.

As suggested by mass spectrometry, this evaluation shows that large clusters with high m/z values contribute the major part of the material flux. Since the ions produced by ESI are only limited in m/z-ratio but not in absolute mass, this implies that much higher deposition rates can be achieved with cluster beams as compared to single molecular ion beams.[8,13] Based on the values for the average m/z-ratio obtained from the first deposition experiments, we are able to quantify the deposition rate. For our sample area of 12.5 mm^2 and deposition currents of up to 250 pA a completely closed double membrane layer requires a deposited charge of 346 pAh, hence multilayered films are fabricated within a few hours.

Using AFM on graphite and SiO_x we found SDS films of submonolayer up to multilayer coverage (**Figures 2** and **3**). The films were stable in air on the timescale of days when gentle scanning conditions are applied (for details see supplementary information V). The main features observed on graphite and SiO_x surfaces are flat compact islands of (3.7 ± 0.4) nm height (Figures 2 and 3). They develop at submonolayer coverage (Figures 2a and 3a) and continue to grow as stacked layers of uniform height with increasing

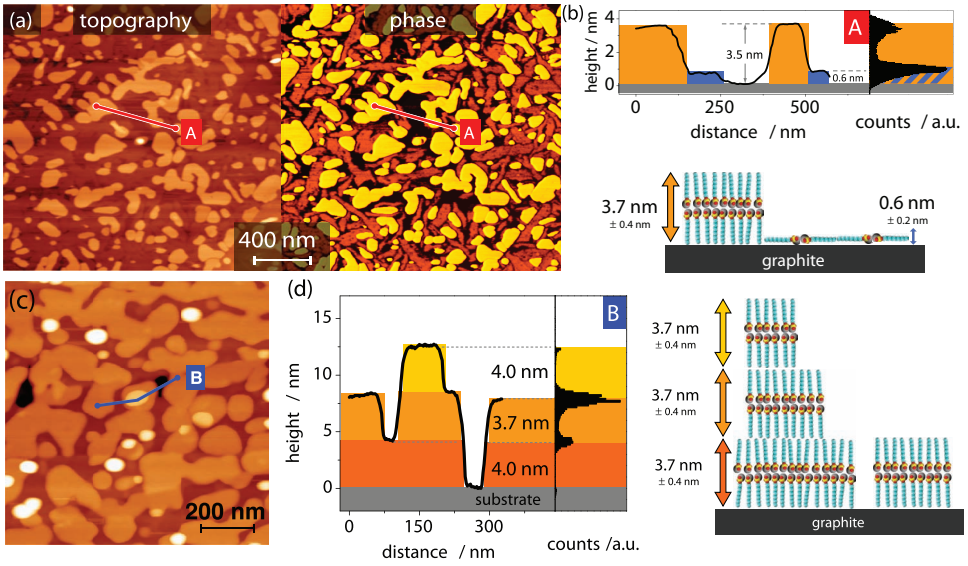

Figure 2. SDS layers on graphite. a) AFM topography and phase image showing two types of domains at submonolayer coverage. b) Cross section (indicated A) and height histogram. Tentative molecular model for SDS sub-monolayers. c) AFM topography of multilayer coverage of SDS on graphite. d) Cross section (indicated B) and height histogram. Schematic model of the multilayer molecular structure.

coverage (Figures 2c and 3b). On graphite an additional type of (0.6 ± 0.2) nm high domain is observed amidst the dominating higher islands, which can be best observed in the AFM phase image (Figure 2a) due to the higher contrast. This second type of island is present at submonolayer coverage but disappears at higher coverage. Similar domains are most probably present also on SiO_x, although a direct imaging by AFM is hindered by the roughness of the amorphous substrate. A closed molecular layer of about 0.6 nm height could in fact explain why the first SDS terrace on SiO_x is found to be consistently lower than the successive ones at a value of (3.0 ± 0.4) nm (Figure 3c).

The island distribution on both, graphite and SiO_x, substrates is homogeneous in size and density over the entire width of the sample. This indicates growth from a well-defined ion beam, delivering SDS cluster ions homogeneously distributed across the surface. In particular the deposition of droplets can be excluded, since this would lead to an inhomogeneous material distribution, characteristic for shattered, dried up droplets (shown in supporting information VI, Figure S2). The observed islands are thus the result of diffusion and agglomeration and their large lateral dimension of 50–500 nm on both substrates suggests a significant surface mobility of the deposited material.

At submonolayer coverage the SDS islands exhibit a well-defined, characteristic morphology with straight edges on both *SiO_x* and graphite, indicative of crystallinity. Suggested by the morphology of the film in Figure 2a, upon coalescence the domains keep their orientation, and thus the resulting closed film is expected to be polycrystalline. Islands with straight edges are particularly pronounced at low coverage for both phases on graphite (**Figure 2**a and 4b) while, at higher coverage, rounded islands can be observed in the elevated layers of the SDS-film (Figure 2c). The domain edges are found to align with the three principal crystallographic directions of the graphite surface forming characteristic angles of 120° between them (Figure 4b). On the contrary, the amorphous SiO_x surface does not select any specific edge direction and the islands tend to have a more rounded morphology at submonolayer coverage (Figure 3a), while only in higher layers straight edges can occasionally be found (see inset Figure 3b).

To determine the molecular interactions responsible for the structure of the fabricated films it is helpful to compare the island morphology observed by AFM (Figures 2 and 3) to the anhydrous forms of bulk SDS crystals grown from solution.[14,15] All SDS crystals grown in solution have the shape of {100}-oriented platelets with alternating polar and apolar regions typical of surfactant bilayers, where molecules are ordered in a head-to-head and tail-to-tail manner.[14] Within each layer the molecule's main axis is oriented almost perpendicular to the {100} face so that the spacing between bilayers is about 3.8 nm. Two major binding forces determine the growth of SDS crystals: ionic/dipole in the polar region and van-der-Waals in the apolar region. The combination of these two interactions in an aqueous medium results in a significantly lower surface energy of the metal-sulfate terminated {100} planes and therefore in the observed plate-like crystal morphology.

The expected lamellar thickness of 3.8 nm agrees well with our observation,[16] indicating that the vacuum-grown SDS structures on graphite and SiO_x can be identified as molecular double layers of upright standing SDS molecules. However, for the bilayers composing the films grown by ES-IBD, we expect an inverse membrane configuration terminated by aliphatic chains (see Figures 2b, 2d and 3d). In fact, due to the missing hydrophilic-hydrophobic interactions, the growth in vacuum is dominated by the ionic/polar interaction between the $NaSO_4$– groups, implying that inverse bilayers are the more stable double layer structure in vacuum.

ADVANCED MATERIALS
www.advmat.de

Materials Views
www.MaterialsViews.com

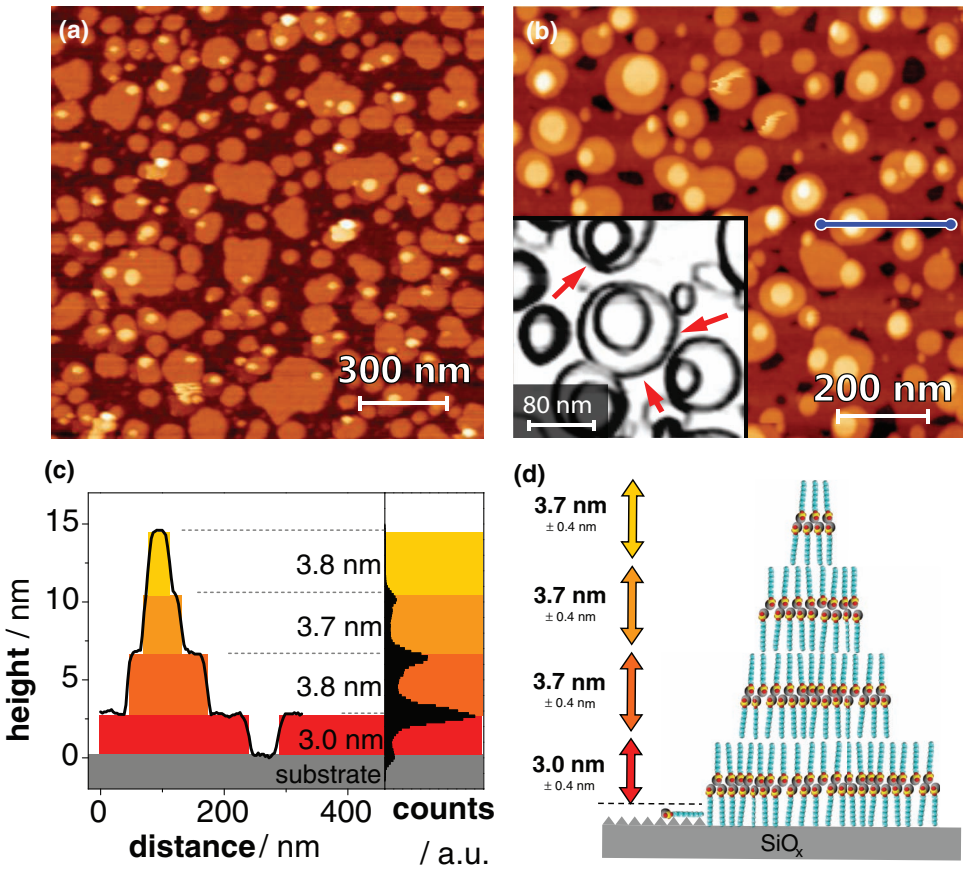

Figure 3. SDS layers on SiO_x a) AFM image at submonolayer coverage. b) AFM image of multilayer SDS islands; cross section indicated. Inset: edge filtered image: red arrows point out straight edges. c) Cross section: first SDS layer (3.0 nm) and 3 stacked double layers (3.7–3.8 nm). The height histogram is derived from the whole AFM image 3b. d) Schematic model of the layer formation for SDS on SiO_x.

To confirm the crystallinity and molecular structure of the films, X-ray powder diffraction (XRPD) measurements were performed on SDS layers on graphite after the deposition of approximately 450 pAh, which corresponds to a coverage of 1.3 monolayers of the upright standing double membrane phase. Under these conditions we still expect the presence both phases—flat laying and upright—at the surface, because in the observed island growth mode higher layers are formed before the first one is closed (see Figure 2c).

Two types of Bragg reflections could be identified in the diffraction pattern: intense peaks belonging to the graphite substrate and a set of reflexes, five orders of magnitude smaller (Figure 4c). Assuming a mixture of 90% 2H and 10% 3R graphite, the intense reflections could be satisfactorily fitted by whole powder pattern fitting (WPPF, see supplementary information IV for details). The Bragg peaks of low intensity mostly belong to (h00) reflections, while mixed indices occur only at higher diffraction angle (marked with † in Figure 4c). Two different SDS phases with slightly different lattice parameters were identified, both showing the characteristic long a-axis of approximately 4 nm, with 0.47 nm and 0.83 nm for *b*- and *c*-axes of a nearly orthorhombic unit cell. These values are similar to the literature values on anhydrous SDS crystals grown from solution (a = 3.91 nm, b = 0.47 nm, a = 0.82 nm),[14,15] and are in agreement with the data obtained from the AFM measurements (3.8 nm height), confirming the crystallinity of the fabricated SDS films on graphite and their membrane-like molecular structure.[17]

While AFM and XRPD measurements explain the structure of the inverse membranes of upright standing molecules, the structure of the layer of flat laying molecules remains to be discussed. The height of 0.6 nm observed by AFM on graphite fits with the size of the a- or b-axes of the bulk phase, supporting the interpretation as a layer of flat laying molecules (see Figure 2). However additional evidence is needed, since no molecular resolution was achieved by ambient condition AFM and moreover the height measured in AFM is an *interaction distance*, given by the range of the force between tip and sample, rather than the actual molecule's size.

Several examples of coatings of flat laying amphiphilic molecules have been reported at liquid-solid interfaces and at surfaces in vacuum.[19] In the following, this possibility is further explored using in-situ scanning tunneling microscopy (STM) to validate our interpretation with high resolution data. A submonolayer coverage of SDS was deposited in UHV on a single-crystal Cu(001) surface. To avoid thick insulating films that would inhibit STM measurements, only a small amount of light SDS clusters (m/z < 5000 Th) were mass-selected and deposited. As already observed on graphite and SiO_x, we find that SDS has an extremely high surface mobility also on

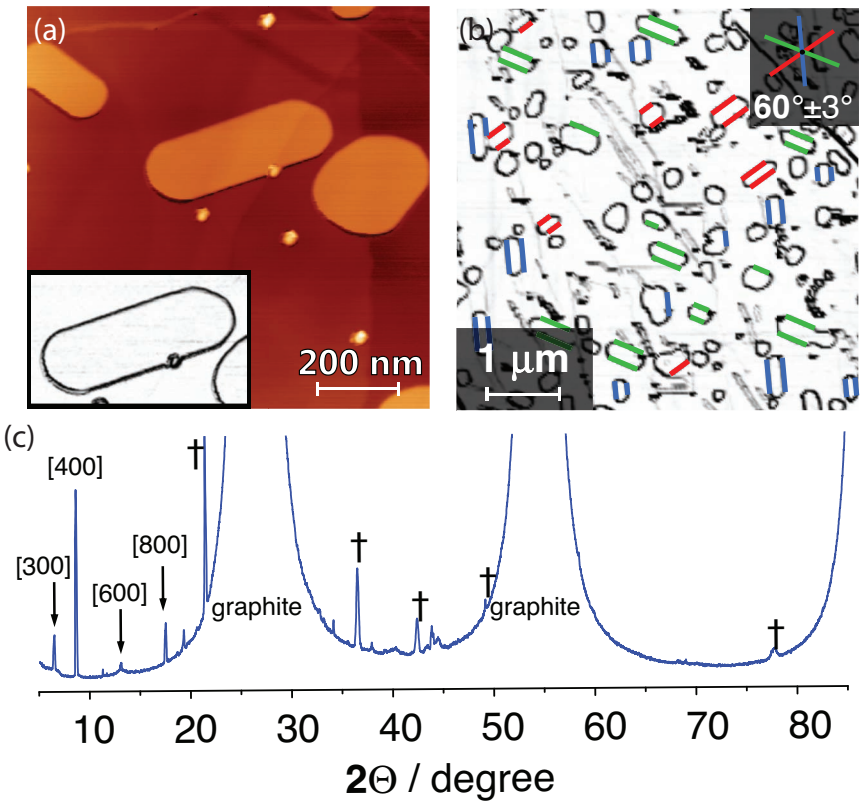

Figure 4. Crystalline ordering in submonolayer coverage of SDS on graphite observed in AFM and XRPD. a) Magnified large islands. The inset shows an edge filtered image, highlighting the facets of the crystallite. b) Edge filtered overview AFM-image. The long parallel edges of the islands follow three preferential growth directions; highlighted by green, red and blue. c) X-ray powder diffraction Θ–2Θ scan of 1.3 monolayer SDS deposited on graphite by ES-IBD in vacuum. Reflexes of the SDS layers are visible on top of an intense signal from the graphite substrate; three peaks at $2\Theta = 26°$, 55° and 87°. Most SDS peaks correspond to scattering from [h00] planes, while some reflexes contain contributions from the a- and b-axes (indicated by †).

Cu(001). Nevertheless, if the measurements are performed at 40 K, the diffusivity is sufficiently inhibited to allow the imaging of stable domains with molecular resolution already at submonolayer coverage. Even at low temperature this is not observed on graphite, indicating a stronger interaction of SDS with the Cu(001) surface.

Figure 5a shows domains of flat-laying SDS molecules adsorbed on Cu(001). The islands have a characteristic elongated shape and grow along four directions separated by 45°. Magnified STM images (Figure 5c) reveal the presence of regular bright lines oriented along the main axis of the islands. Fourier transformed STM images (Figure 5b) reveal a periodicity of (3.4 ± 0.4) nm corresponding to a molecular double row, and (1.7 ± 0.2) nm for the single molecular row respectively, indicated in the tentative model in Figure 5d. Despite the strong binding to the Cu(001) surface, the head-to-head, tail-to-tail alignment of the SDS molecules prevails, further proving that this is the energetically favored configuration. On the two-fold symmetric Cu(001) surface the observed 45° separation between successive island orientations implies that their long axis must be rotated by 22.5° with respect to the [110] and [-110] principal crystallographic directions. Equivalently, the observation of only three domain orientations for the flat laying SDS phase on HOPG suggests that the islands are aligned along the main surface directions of the three-fold symmetric graphite surface (Figure 2a).

The existence of a flat laying phase on copper confirms the interpretation of the 0.6 nm thick domains observed on graphite as being composed by molecules adsorbed parallel to the surface. We expect the formation of a similar phase also on SiO_x, although the higher roughness of this substrate prevents this adlayer from being directly revealed in AFM measurements. Vice versa, we cannot exclude the existence of an upright standing molecular phase on Cu(001), which could however not be imaged in STM. In fact, the fuzziness of the STM images as well as fast tip degradation suggests the presence of either mobile molecules or of upright standing molecular domains with a low tunneling conductance.

It is the hierarchy of molecule-surface and intermolecular interactions that determines the structure, morphology and texture of the SDS crystals on surfaces. The combination of strong attractive interaction between the sodium-sulfonate groups and weak interaction of the lengthy alkyl chains enforces a head-to-head and tail-to-tail ordering. As a consequence, SDS dimers are the basic structural feature in the inverted double layer membranes and the flat laying double row aggregates.

On a subordinated hierarchy level of interaction, the surface influences the packing and ordering of the SDS molecules within the layer. In an ideal double layer system straight SDS molecules are oriented as illustrated in Figures 2b,d and 3d, but the interaction with the substrate could in principle perturb the system. However, a lateral or vertical shift of a SDS molecule from its ideally packed position requires a significant loss of the van der Waals interaction energy due the displacement of eleven internal CH_2 groups, one terminal CH_3 group, and the SO_4 group. This loss of energy cannot be compensated by the non-bonding substrate–SDS molecule interaction, which mainly involves the interaction between the substrate and the terminal CH_3 group. Thus the weak coupling of SDS to the substrates competing with the strong intermolecular interactions of the aligned aliphatic chains leads to the characteristic morphology of the SDS layers growing on graphite, SiO_x and in higher SDS layers. As a direct consequence of this interplay, the upright standing, double layer configuration is preferred on all substrates at sufficient coverage, while the flat laying phase does not continue to grow into the third dimension. The influence of the surface is expressed only through a template effect on the island orientation on the crystalline surfaces of graphite

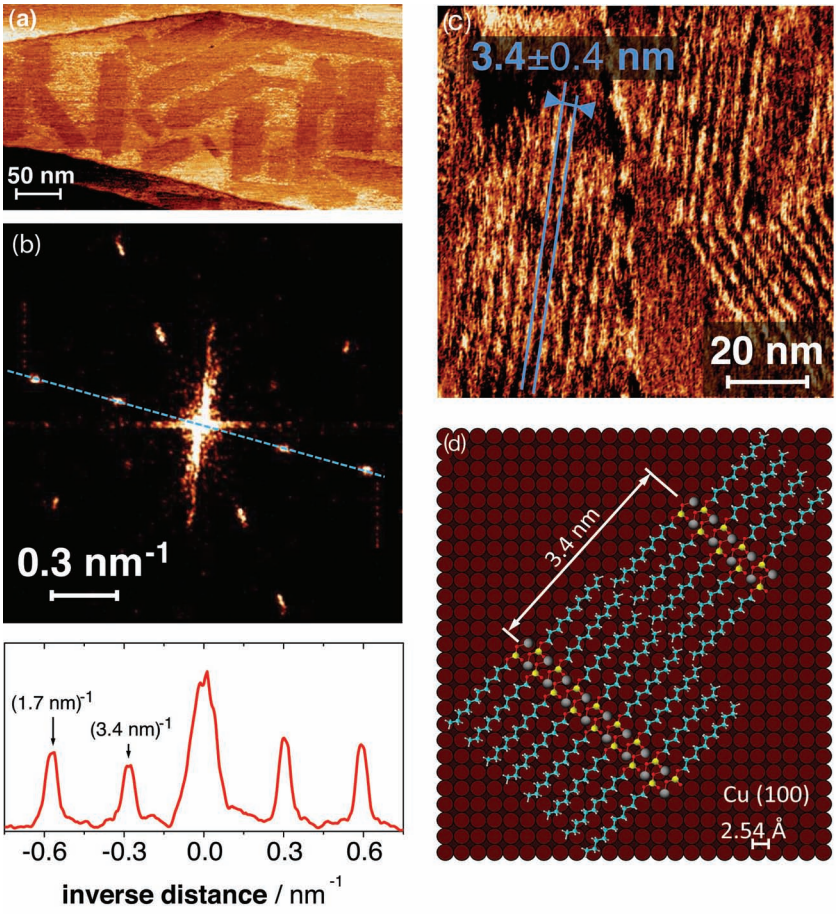

Figure 5. UHV-STM topography of SDS submonolayer on Cu(001) deposited by ES-IBD. (T = 40 K) a) Rod shaped islands following four orientations. (gap voltage −2V, tunneling current 100 pA, a tip artifact possibly caused the inverted contrast.) b) Two dimensional Fourier transformation of SDS islands on Cu(001). Peaks corresponding to single and double rows are visible. Three domains rotated by 45° are visible, the fourth was not present in the STM image (see supporting information **VII**, Figure S3). c) Magnified SDS domain: stripes correspond to double rows of SDS. (bias 2.2 V, tunneling current 100 pA), d) Tentative model of the adsorption geometry.

and copper and in slight deviations from the bulk crystal structure.

In addition, the soft deposition of large inverse micelle clusters might further influence the structure formation. Clusters adsorbed in this configuration have the aliphatic chains pointing to the outside where they bind weakly to the substrate surface. We hypothesize that large clusters stay intact during deposition, are mobile as whole entity and preferably fuse into larger islands of upright standing SDS molecules in inverse membrane configuration.

In summary, ion beam deposition proves to be a suitable tool for the growth of crystalline thin films of nonvolatile molecules at surfaces. The deposition of SDS cluster ion beams on solid surfaces in vacuum results in stable molecular films. Inverted double-membranes as well as a flat laying phase were obtained, all exhibiting characteristic features of crystalline ordering, such as a constant layer thickness, low roughness, and characteristic domain shapes. The hydrophilic-hydrophobic interaction is not present in a vacuum environment, yet the hierarchy of bond strength given by the molecular structure of the amphiphiles leads to the growth of nanostructures that still arrange into a head-to-head and tail-to-tail configuration.

Only few methods to deposit unsublimable molecules in vacuum exist as an alternative to the presented ES-IBD scheme.[20] Ordered molecular structures were so far only demonstrated by matrix-assisted laser desorption ionization (MALDI) ion beam deposition of insoluble molecules[21] or by the direct injection of an electrospray into a differentially pumped vacuum apparatus without using mass filters or ion optics.[22] A great deal of large functional molecules are made via solution based organic synthesis or are of biological origin and are thus necessarily soluble. For example, proteins and peptides, both easily ionized in ESI, represent vast classes of functional molecules. Well-defined crystalline films from such soluble yet nonvolatile molecules can now be prepared by ES-IBD on technologically relevant surfaces which can even be insulating, as shown for SiO_x. Thus ES-IBD represents a hybrid technology useful for top-down and bottom-up approaches. It can be used to fabricate thin films on a macroscopic scale that could be structured by top-down techniques, and as well to deposit complex functional entities, that self-assemble into nanostructures from bottom up.

In comparison to other ion beam deposition techniques, ES-IBD has the advantage of an intense, continuous, fully controlled beam, allowing to deposit with reasonable rates. Up to one monolayer per hour per square centimeter is possible, which could even be increased using cluster beams as presented here. In general, the use of charged particles or cluster beams is an additional advantage since it allows to use ion optics to pattern the deposition or to exploit reactive landing[7] to fabricate materials that could not be grown ex situ or through conventional vacuum processing. Furthermore, the presented cluster deposition approach suggests another possibility of ES-IBD, which is the vacuum deposition of nanoparticles, which are generally nonvolatile. In fact our deposition experiments show that the average SDS cluster contains 17 molecules per charge and carries 25 charges. This aggregate of 425 molecules has a mass 1.2×10^5 u and a diameter of 7 nm and as such represents what is defined as a nanoparticle.[11] Hence, this work demonstrates the possibility to charge nanoparticles highly and use them like a molecular cluster ion beam for analytical and preparative applications.

Experimental Section

All samples are prepared by electrospray ion beam deposition (ES-IBD) of sodium-dodecyl-sulfate (SDS) cluster beams in (ultra-)high

vacuum (see supporting information **I**). ES-IBD as a method to deposit nonvolatile materials on solid surfaces in vacuum has been developed recently.[3,6,23] In our laboratory we set up an instrument that is designed particularly for vacuum deposition under highly controlled conditions as described in detail elsewhere.[4,6]

Silicon (SiO_x, 1–2 nm native oxide) and graphite surfaces are prepared ex situ and placed in high vacuum for deposition and analyzed by tapping mode atomic force microscopy (AFM) in air. X-ray powder diffraction (XRPD) measurements were performed ex situ with graphite samples. The copper surface Cu(001) is prepared in situ under ultrahigh vacuum (UHV) conditions, transferred in situ to the deposition and back to the scanning tunneling microscope (STM) for analysis.

Supporting Information

Supporting Information is available from the Wiley Online Library or from the author.

Acknowledgements

The authors thank M. F. Schneider, S. Stepanow and F. Rosei for fruitful discussions. S.R. was supported by the Hans-L.-Merkle Foundation for excellence in science.

Received: December 14, 2011
Published online: April 20, 2012

[1] a) A. Ulman, *Chem. Rev.* **1996**, *96*, 1533–1554; b) C. Dimitrakopoulos, P. Malenfant, *Adv. Mater.* **2002**, *14*, 99; c) M. Halik, H. Klauk, U. Zschieschang, G. Schmid, C. Dehm, M. Schtz, S. Maisch, F. Effenberger, M. Brunnbauer, F. Stellacci, *Nature* **2004**, *431*, 963–966; d) S. Reineke, F. Lindner, G. Schwartz, N. Seidler, K. Walzer, B. Luessem, K. Leo, *Nature* **2009**, *459*, 234.

[2] J. B. Fenn, M. Mann, C. K. Meng, S. F. Wong, C. M. Whitehouse, *Science* **1989**, *246*, 64–71.

[3] Z. Ouyang, Z. Takats, T. A. Blake, B. Gologan, A. J. Guymon, J. M. Wiseman, J. C. Oliver, V. J. Davisson, R. G. Cooks, *Science* **2003**, *301*, 1351–1354.

[4] S. Rauschenbach, R. Vogelgesang, N. Malinowski, J. W. Gerlach, M. Benyoucef, G. Costantini, Z. Deng, N. Thontasen, K. Kern, *ACS Nano* **2009**, *3*, 2901–2910.

[5] G. E. Johnson, Q. Hu, J. Laskin, *Annu. Rev. Anal. Chem.* **2011**, *4*, 83–104.

[6] S. Rauschenbach, F. L. Stadler, E. Lunedei, N. Malinowski, S. Koltsov, G. Costantini, K. Kern, *Small* **2006**, *2*, 540–547.

[7] P. Wang, J. Laskin, *Angew. Chem., Int. Ed.* **2008**, *47*, 6678–668.

[8] N. Thontasen, G. Levita, N. Malinowski, Z. Deng, S. Rauschenbach, K. Kern, *J. Phys. Chem. C* **2010**, *114*, 17768–17772.

[9] S. D. Hanton, *Chem. Rev.* **2001**, *101*, 527–569.

[10] a) G. Giorgi, E. Giocaliere, L. Ceraulo, A. Ruggirello, V. T. Liveri, *Rapid Commun. Mass Spectrom.* **2009**, *23*, 2206-2212; b) M. Sharon, L. L. Ilag, C. V. Robinson, *J. Am. Chem. Soc.* **2007**, *129*, 8740–8746.

[11] G. Rinke, S. Rauschenbach, T. Weitz, N. Malinowski, N. Thontasen, Z. Deng, L. Harnau, K. Kern, **2011**, unpublished.

[12] U. Zimmermann, N. Malinowski, U. Naher, S. Frank, T. P. Martin, *Z. Phys. D - Atoms Molecules and Clusters* **1994**, *31*, 85–93.

[13] Q. Hu, P. Wang, P. L. Gassman, J. Laskin, *Anal. Chem.* **2009**, *81*, 7302–7308.

[14] L. A. Smith, A. Duncan, G. B. Thomson, K. J. Roberts, D. Machin, G. McLeod, *J. Crystal Growth* **2004**, *263*, 480.

[15] L. A. Smith, G. B. Thomson, K. J. Roberts, D. Machin, G. McLeod, *Crystal Growth and Design* **2005**, *5*, 2164.

[16] L. A. Smith, R. Hammond, K. J. Roberts, D. Machin, G. McLeod, *J. Mol. Struct.* **2000**, *554*, 173–182.

[17] A. Le Bail, H. Duroy, J. L. Fourquet, *Mater. Res. Bull.* **1988**, *23*, 447.

[18] R. W. Cheary, A. A. Coelho, J. P. Cline, *J. Res. Natl. Inst. Stand. Technol.* **2005**, *109*, 1–25.

[19] a) X.-L. Yin, L.-J. Wan, Z.-Y. Yang, J.-Y. Yu, *Appl. Surface Sci.* **2005**, *240*, 13-18; b) A. Langner, S. L. Tait, N. Lin, R. Chandrasekar, M. Ruben, K. Kern, *Angew. Chem., Int. Ed.* **2008**, *47*, 8835-8838; c) S. Sek, M. Chen, C. L. Brosseau, J. Lipkowski, *Langmuir* **2007**, *23*, 12529–12534.

[20] a) A. Rouhanipour, M. Roy, X. Feng, H.-J. Räder, K. Müllen, *Angew. Chem., Int. Ed.* **2009**, *48*, 4602-4604, b) J. C. Swarbrick, J. Ben Taylor, J. N. O'Shea, *Appl. Surf. Sci.* **2006**, *252*, 5622–5626.

[21] H. J. Räder, A. Rouhanipour, A. M. Talarico, V. Palermo, P. Samori, K. Müllen, *Nat. Mater.* **2006**, *5*, 276–280.

[22] A. Saywell, J. K. Sprafke, L. J. Esdaile, A. J. Britton, A. Rienzo, H. L. Anderson, J. N. O'Shea, P. H. Beton, *Angew. Chem., Int. Ed.* **2010**, *49*, 9136–9139.

[23] S. A. Miller, H. Luo, S. J. Pachuta, R. G. Cooks, *Science* **1997**, *275*, 1447–1450.